International Journal of Nanomedicine

Dovepress
Taylor & Francis Group

Open Access Full Text Article

ORIGINAL RESEARCH

Inhalable Albumin Nanoparticles Co-Delivering Dihydroartemisinin and Nintedanib Attenuate Pulmonary Fibrosis by Suppressing TGF-β1/Smad2/3 Signaling

Caopei Zheng[1,2,*], Wei Ding[3,*], Yuqing Sun[1,2], Yu Wang[1], Yulin Zhang[1,2,4]

[1]Department of Respiratory and Critical Care Medicine, Beijing Youan Hospital, Capital Medical University, Beijing, People's Republic of China; [2]Laboratory for Clinical Medicine, Capital Medical University, Beijing, People's Republic of China; [3]Clinical Trial Institution Office, Beijing Jishuitan Hospital, Capital Medical University, Beijing, People's Republic of China; [4]Beijing Research Center for Respiratory Infectious Diseases, Beijing, People's Republic of China

*These authors contributed equally to this work

Correspondence: Yulin Zhang, Department of Respiratory and Critical Care Medicine, Beijing Youan Hospital, Capital Medical University, 8 Xitoutiao, Youanmenwai, Fengtai District, Beijing, People's Republic of China, Tel +86)10-83997143, Fax +86 10-63293371, Email yulinzhang@ccmu.edu.cn

Purpose: Pulmonary fibrosis (PF) is a progressive interstitial lung disease characterized by high morbidity and limited treatment options. Current antifibrotic agents, such as pirfenidone and nintedanib (NIN), are restricted by systemic toxicity and insufficient pulmonary targeting. This study aimed to develop an inhalable human serum albumin (HSA)-based nanoparticle system co-delivering NIN and dihydroartemisinin (DHA), termed DHA/NIN@HSA, to achieve efficient lung-targeted combinational therapy against PF.

Methods: DHA/NIN@HSA nanoparticles were prepared via a self-assembly strategy and characterized for morphology, particle size, and drug-loading efficiency. Pulmonary deposition and retention profiles after airway inhalation were evaluated using in vivo fluorescence imaging. The antifibrotic efficacy and safety of DHA/NIN@HSA were further assessed in a bleomycin-induced PF mouse model.

Results: DHA/NIN@HSA nanoparticles exhibited uniform particle size (125 ± 5 nm) and excellent pulmonary deposition, ensuring prolonged lung retention and reduced systemic exposure. Airway administration of DHA/NIN@HSA every 48 h significantly mitigated fibrosis progression, improved survival, and restored alveolar architecture. Mechanistically, NIN inhibited fibroblast proliferation and myofibroblast differentiation, while DHA suppressed transforming growth factor-β1 (TGF-β1)/Smad2/3 signaling and inflammatory cytokines expression. Notably, DHA showed antifibrotic efficacy comparable to NIN with superior anti-inflammatory activity, highlighting its therapeutic potential in PF.

Conclusion: Airway co-delivery of DHA/NIN@HSA achieved maximal antifibrotic efficacy, precise lung targeting, and favorable safety, providing a translatable nanotherapeutic platform for combinational therapy of PF.

Keywords: inhalable nanoparticles, albumin carrier, pulmonary fibrosis, dihydroartemisinin, nintedanib

Introduction

Pulmonary fibrosis (PF) is a chronic and progressive interstitial lung disease characterized by excessive activation of fibroblasts and abnormal deposition of extracellular matrix (ECM).[1,2] Its global incidence has been steadily increasing, affecting up to 10 individuals per 100,000 population,[3] with an average survival time of only 3–5 years.[4] Epidemiological data indicate that the mortality rate of PF exceeds 20% in the United States and Australia and can reach as high as 80% among elderly patients.[5,6] Thus, PF poses a serious threat to human health and constitutes a major public health challenge demanding urgent solutions.

https://doi.org/10.2147/IJN.S576680
Received: 8 November 2025
Accepted: 13 February 2026
Published: 26 February 2026

Graphical Abstract

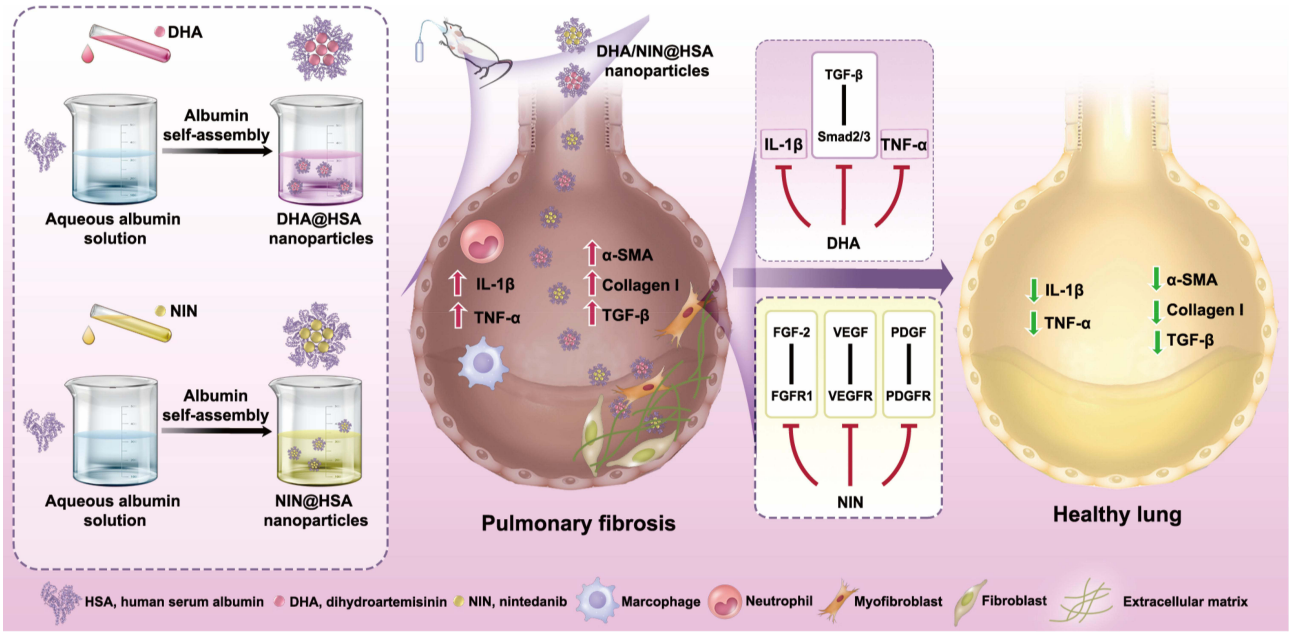

Currently, pirfenidone (PFD) and nintedanib (NIN) are the only antifibrotic agents approved by the United States Food and Drug Administration (FDA) for clinical use. PFD primarily exerts antifibrotic effects by suppressing transforming growth factor-β (TGF-β) signaling, thereby inhibiting fibroblast proliferation and collagen synthesis.[7–9] NIN, a small-molecule tyrosine kinase inhibitor, targets multiple profibrotic pathways including platelet-derived growth factor (PDGF), vascular endothelial growth factor (VEGF), and fibroblast growth factor (FGF), collectively attenuating fibroblast activation and differentiation.[10,11] Despite their clinical benefits, both drugs only slow disease progression without significantly reducing mortality, and their use is often limited by gastrointestinal disturbances and hepatotoxicity.[12–14] Therefore, there is an urgent need for novel therapeutic strategies that enhance efficacy while minimizing systemic toxicity.

Dihydroartemisinin (DHA), a semi-synthetic derivative of artemisinin, has been widely employed as an antimalarial agent and has recently garnered increasing attention for its potential antifibrotic activity. Previous studies have demonstrated that DHA effectively alleviates bleomycin (BLM)-induced PF, which has been attributed to its ability to suppress inflammatory cytokines (eg, TNF-α) and inhibit the TGF-β1/Smad2/3 signaling pathway—a critical axis driving fibroblast activation and ECM accumulation.[15–17] Notably, this mechanism complements that of NIN. Specifically, NIN predominantly inhibits multiple receptor tyrosine kinases (PDGFR, VEGFR, and FGFR) to suppress fibroblast proliferation and profibrotic signaling, whereas DHA modulates the TGF-β1/Smad2/3 axis and inflammation-associated pathways to limit myofibroblast differentiation and cytokine release. Given that PF progression involves both proliferative and inflammatory drivers, co-targeting these complementary pathways may provide enhanced therapeutic benefit and potentially synergistic effects compared with monotherapy.

In clinical practice, NIN and PFD are predominantly administered orally. However, this route is limited by extensive first-pass metabolism, delayed onset of action, low pulmonary bioavailability, and systemic adverse effects (AEs) such as diarrhea and hepatotoxicity.[18,19] Simply increasing the oral dose does not ensure sufficient drug accumulation in the lungs and may further increase the risk of hepatic and renal toxicity. In contrast, inhalation delivery enables direct deposition of therapeutic agents into the lungs, potentially increasing local drug exposure while reducing systemic distribution.

However, achieving sufficient pulmonary retention and sustained therapeutic levels remains a key challenge for inhalable formulations.

Indeed, inhaled antifibrotic strategies have progressed into clinical and preclinical development. A Phase 1b trial of inhaled PFD solution (AP01) in patients with idiopathic PF reported improved tolerability compared with oral therapy, supporting the translational feasibility of pulmonary antifibrotic delivery.[20] In parallel, preclinical studies have shown that spray-dried inhalable NIN dry powders can achieve efficient lung deposition.[21] Nevertheless, inhaled small-molecule formulations may still require repeated administration and can be constrained by pulmonary clearance and limited local residence time. These limitations underscore the need for advanced inhalable carrier platforms capable of enhancing lung retention and sustaining local drug availability.

In this context, the development of a suitable nanocarrier system is crucial to improve pulmonary retention and sustain local drug availability after inhalation delivery. Human serum albumin (HSA), an endogenously abundant and biocompatible protein, has emerged as a versatile drug delivery vehicle due to its excellent safety profile, prolonged circulation, and multiple hydrophobic binding sites that facilitate drug encapsulation.[22,23] For instance, encapsulation of the poorly soluble artemisinin derivative artemether into HSA nanoparticles markedly enhanced its aqueous solubility by nearly 50-fold.[24] Such evidence supports the feasibility of HSA-based nanoparticles as ideal carriers for lipophilic drugs such as DHA and NIN.

In summary, DHA and NIN exert antifibrotic effects through complementary mechanisms, yet their clinical application is limited by the drawbacks of oral administration. To overcome these challenges, we developed an inhalable HSA-based nanoparticle system co-delivering DHA and NIN (DHA/NIN@HSA). This formulation enables efficient pulmonary deposition, enhances inhibition of TGF-β1/Smad2/3 signaling, and reduces systemic exposure, providing a safer, effective, and clinically translatable strategy for PF.

Materials and Methods

Materials and Reagents

DHA was purchased from Selleck (Houston, TX, USA). NIN was kindly provided by Qilu Pharmaceutical Co., Ltd. HSA, anhydrous ethanol, and dimethyl sulfoxide (DMSO) were obtained from Sigma-Aldrich (St. Louis, MO, USA). Dulbecco's Modified Eagle Medium (DMEM, high glucose) and fetal bovine serum (FBS) were supplied by Thermo Fisher Scientific (Waltham, MA, USA). Trypsin–Ethylenediaminetetraacetic acid (EDTA) and penicillin–streptomycin solutions were obtained from VivaCell Biotechnology Co., Ltd. (Shanghai, China). TGF-β1 (HY-P70648) and Cell Counting Kit-8 (CCK-8, HY-K0301) were purchased from MedChemExpress (MCE, USA).

Primary antibodies, including anti-Collagen I (ab316222), anti-α-smooth muscle actin (α-SMA) (ab7817), Alexa Fluor® 488 conjugated anti-mouse IgG (ab150117), and Alexa Fluor® 647 conjugated anti-rabbit IgG (ab150079), were purchased from Abcam (Cambridge, UK). Antibodies against TGF-β1 (Cat. No. 3711S), Smad2/3 (Cat. No. 8685T), and phosphorylated Smad2/3 (p-Smad2/3; Cat. No. 8828T) were obtained from Cell Signaling Technology (Danvers, MA, USA). GAPDH mouse monoclonal antibody (AG019), β-Tubulin mouse monoclonal antibody (AF2839), and the BeyoColor™ Prestained Protein Marker (P0071, 6.5–270 kDa) were obtained from Beyotime Biotechnology (Shanghai, China). Horseradish peroxidase (HRP)-conjugated secondary antibodies, including goat anti-rabbit IgG (bs-0295G-HRP) and goat anti-mouse IgG (bs-0296G-HRP), were purchased from Bioss Co., Ltd. (Beijing, China). Enzyme-linked immunosorbent assay (ELISA) kits for interleukin-1β (IL-1β) (BMS6002-2), tumor necrosis factor-α (TNF-α) (BMS607-3), and TGF-β1 (BMS608-4) were purchased from Thermo Fisher Scientific. The hydroxyproline (HYP) assay kit was obtained from Solarbio (Beijing, China; Cat. No. BC0250). Unless otherwise specified, all other reagents were of analytical grade and obtained from Sigma-Aldrich.

Cell Culture and Animal Experiments

NIH/3T3 fibroblasts (Procell Life Science & Technology, Wuhan, China; Cat. No. GCL-0171) were cultured in DMEM supplemented with 10% FBS and 1% penicillin–streptomycin at 37°C in a humidified incubator with 5% CO_2. Male C57BL/6 mice (6–8 weeks, 20 ± 2 g, specific pathogen free grade) were obtained from Shenzhen Maike Biotechnology

Co., Ltd. (Shenzhen, China). All animals were cared for according to the Guidelines for the Ethical Review of Laboratory Animal Welfare (GB/T 35892–2018). Experimental procedures were approved by the Institutional Animal Care and Use Committee of the Institute of Process Engineering, Chinese Academy of Sciences (IPEAECA2024031).

Preparation and Characterization of DHA@HSA and NIN@HSA Nanoparticles

DHA (25 mg/mL) and NIN (100 mg/mL) stock solutions were first prepared by dissolving each compound in DMSO under ultrasonication (room temperature, 10 min). HSA solution (1 mg/mL) was prepared by dissolving 30 mg HSA in 30 mL deionized water, followed by sonication in a water bath (100 W, 30 min) to ensure complete dissolution. Nanoparticles were synthesized using a desolvation/antisolvent-induced self-assembly approach. Briefly, 400 μL of DHA stock or 200 μL of NIN stock solution was separately diluted in 4 mL of anhydrous ethanol and sonicated until fully dissolved. The ethanolic drug solution was then added dropwise into 4 mL of HSA solution under continuous sonication (water bath, 100 W), followed by an additional 30 min of sonication to promote nanoparticle formation. The suspensions were centrifuged at 10,000 × g for 8 min, and the precipitates were collected and re-dispersed in 1 mL deionized water. Particle size and zeta potential were analyzed by dynamic light scattering (DLS), while drug concentrations were determined using high-performance liquid chromatography (HPLC) and ultraviolet–visible (UV–Vis) spectrophotometry, respectively. The morphology of the nanoparticles was further examined using transmission electron microscopy (TEM).

Colloidal Stability of DHA@HSA and NIN@HSA Nanoparticles

The colloidal stability of DHA@HSA and NIN@HSA nanoparticles was evaluated in phosphate-buffered saline (PBS, pH 7.4). Nanoparticle suspensions were incubated at 37 °C, and hydrodynamic diameter and polydispersity index (PDI) were measured at predetermined time points (0, 12, 24, 36, and 48 h) using dynamic light scattering. Measurements were performed in triplicate, and data are presented as mean ± standard deviation.

In vitro Drug Release Study

The in vitro release profiles of DHA and NIN from DHA/NIN@HSA nanoparticles were evaluated using the dialysis bag method. Briefly, 2.0 mL of nanoparticle dispersion was transferred into a sealed dialysis bag with a molecular weight cut-off (MWCO) of 10 kDa. The dialysis bag was immersed in 20 mL of PBS (pH 7.4) containing 0.1% (v/v) Tween 80 to maintain sink conditions. The system was incubated at 37°C in a thermostatic shaker with gentle agitation (100 rpm). At predetermined time points (3, 12, 24, and 48 h), 1.0 mL of the release medium was withdrawn and immediately replaced with an equal volume of pre-warmed fresh medium. The concentrations of DHA and NIN in the collected samples were quantified by HPLC and UV–Vis spectrophotometry, respectively. All experiments were performed in triplicate.

Quantification of DHA and NIN in Lung Tissue

At 12, 24, and 48 h after intratracheal administration, mice were euthanized and the entire lungs were harvested. The lungs were gently blotted dry with lint-free tissue and weighed (W, mg). A fixed volume of extraction solvent (V_{ext} = 1.00 mL) was added to each lung sample, followed by homogenization on ice. The homogenates were centrifuged at 4°C (10,000 × g, 5 min), and the clarified supernatants were collected for drug quantification. If the drug concentration exceeded the linear range of the calibration curve, the supernatants were diluted with PBS, and the dilution factor (DF) was recorded.

DHA concentrations were determined using a HPLC system. Quantification was performed using an external standard calibration curve. DHA standard solutions were prepared at graded concentrations (1.0, 0.5, 0.25, 0.0625, and 0.0078 mg/mL). Peak areas were plotted against the corresponding standard concentrations, and linear regression was applied to obtain the calibration equation and coefficient of determination (R^2). DHA concentrations in the lung extracts (C_{ext}, mg/mL) were calculated from the calibration equation and corrected for dilution when applicable ($C_{ext} = C_{meas} \times DF$). Specificity was verified by analyzing blank lung homogenates, confirming the absence of interfering peaks at the retention time of DHA.

Similarly, NIN concentrations were determined by UV–Vis spectrophotometry. Briefly, a series of NIN standard solutions were prepared to generate the calibration curve, and absorbance was measured at 385 nm. Sample concentrations were calculated from the corresponding absorbance values (with dilution when necessary). Blank lung homogenate extracts were used for background subtraction.

Calculation of DHA and NIN Amounts in Lung and Pulmonary Retention (%)

The total amount of drug in the whole lung at each time point (A_{lung}, mg) was calculated using the following equation: $A_{lung} = C_{ext} \times V_{ext}$, where C_{ext} represents the drug concentration in the lung extract (mg/mL), and V_{ext} is the fixed extraction volume (1.00 mL). Pulmonary retention of each drug was expressed as percentage of the administered dose (% ID) and calculated as follows: Drug retention (%ID) = $(A_{lung}/D_{admin}) \times 100\%$, where D_{admin} (mg) denotes the total administered dose per mouse. For DHA, D_{admin} was calculated based on the dosing regimen (2 mg/kg) and an average body weight of 20 g, yielding 0.04 mg per mouse. For NIN, D_{admin} was calculated based on the dosing regimen (4 mg/kg) and an average body weight of 20 g, yielding 0.08 mg per mouse. All experiments were performed in triplicate.

Cell Viability Assay

Cell viability was assessed using CCK-8 assay. NIH/3T3 cells were seeded in 96-well plates (1×10^4 cells/well) and incubated overnight. The culture medium was then replaced with fresh medium containing TGF-β1 (10 ng/mL) and various concentration combinations of co-delivered DHA@HSA and NIN@HSA nanoparticles (corresponding to equivalent drug concentrations of DHA and NIN), followed by incubation for 48 h. Untreated cells served as the control group. Cell viability was determined by measuring absorbance at 450 nm using a microplate reader.

Immunofluorescence Staining

NIH/3T3 cells were cultured on confocal dishes (Solarbio, YA0570) and treated with TGF-β1 (10 ng/mL) in the presence of NIN or DHA for 48 h. Cells were then washed with PBS, fixed with 4% paraformaldehyde for 20 min, permeabilized with 0.1% Triton X-100 for 10 min, and blocked with 10% goat serum for 30 min at room temperature. Cells were incubated overnight at 4 °C with primary antibodies against Collagen I (1:100) and α-SMA (1:100), followed by Alexa Fluor® 488– or Alexa Fluor® 647–conjugated secondary antibodies (1:200, 30 min, room temperature). Nuclei were stained with Hoechst 33342 (1:100, 15 min). Fluorescence images were captured using a Nikon Eclipse Ti2 inverted microscope equipped with an A1 confocal laser scanning system (Nikon, Japan).

Western Blotting

Protein expression of fibrosis-related markers (α-SMA, Collagen I, TGF-β1, Smad2/3, and p-Smad2/3) was analyzed by Western blotting (WB). Lung tissues were homogenized in radioimmunoprecipitation assay (RIPA) buffer containing protease inhibitors, lysed on ice, and centrifuged. Protein concentrations were determined by bicinchoninic acid (BCA) Assay. Equal amounts of protein were separated by SDS–PAGE, transferred onto PVDF membranes, and blocked in 5% nonfat milk. Membranes were incubated with primary antibodies (1:1000) overnight at 4 °C and then with HRP-conjugated secondary antibodies (1:5000) for 1 h. Bands were visualized using enhanced chemiluminescence (ECL) and quantified with ImageJ software.

Animal Model and Treatment

PF was induced in C57BL/6 mice by intratracheal instillation of BLM (2.5 mg/kg) using a microsprayer (Penn-Century, USA) under anesthesia induced by intraperitoneal injection of 1% pentobarbital sodium (50 mg/kg). Seven days after BLM instillation, mice were randomly assigned to five groups: (1) PBS, (2) BLM, (3) NIN@HSA, (4) DHA@HSA, and (5) DHA/NIN@HSA. Treatments were administered intratracheally every 48 h for a total of seven treatments. The doses of DHA (2 mg/kg) and NIN (4 mg/kg) were selected based on previous inhalation studies[25,26] and our preliminary in vitro pharmacodynamic evaluation, aiming to achieve effective pulmonary exposure while minimizing systemic toxicity.

Given the expected mortality in the BLM model, three parallel sets of experiments were conducted under identical conditions (modeled and treated on the same day using the same reagent batches), with 6 mice per group in each set. One set of mice (n = 6 per group) was predefined for survival analysis, and survival time was recorded only for this cohort. The remaining sets were used for endpoint analyses. At Day 21, 6 mice per group (including the BLM group) were randomly selected from the pooled animals across these sets, euthanized, and lung tissues, serum, and bronchoalveolar lavage fluid (BALF) were collected for downstream analyses.

Micro-CT Imaging

Micro-computed tomography (micro-CT) imaging was performed using a Revvity system under standardized conditions (70 kV, 80 μA, voxel size = 40 μm, FOV = 20 mm, scan duration = 4.5 min). Mice were anesthetized and scanned in the supine position. Three-dimensional (3D) reconstruction and quantitative analysis were performed using Analyze 14.0 software with identical parameters applied across all samples.

Serum and BALF Collection

On day 21, blood samples were collected, allowed to clot at room temperature for 2 h, and then centrifuged at 1500 × g for 15 min at 4 °C to obtain serum. Serum alanine aminotransferase (ALT), aspartate aminotransferase (AST), and blood urea nitrogen (BUN) levels were measured to assess systemic toxicity. BALF was obtained by inserting a 1 mL syringe containing PBS into the exposed trachea and flushing the lungs three times (total 1.5 mL). The collected fluid was pooled, centrifuged at 400 × g for 8 min, and the supernatant was used for protein assays.

Histological Analysis

After treatment, the lungs, heart, liver, spleen, and kidneys were collected for histological evaluation. Lung tissues were fixed in 4% paraformaldehyde for 24 h, embedded in paraffin, sectioned at 4 μm thickness, and stained with hematoxylin–eosin (H&E) and Masson's trichrome (MT) to assess inflammatory infiltration and collagen deposition. Other major organs were stained with H&E to evaluate systemic toxicity. The degree of PF was semi-quantitatively assessed using the modified Ashcroft scoring system: 0 = normal; 1 = minimal fibrous thickening of alveoli or bronchioles; 2–3 = moderate alveolar wall thickening without marked structural damage; 4–5 = distinct architectural distortion with formation of fibrous bands or small fibrotic foci; 6–7 = severe destruction with honeycomb-like changes; and 8 = complete fibrotic obliteration.

ELISA Assay

Lung tissues were weighed and homogenized in 1 mL of PBS using a Bead Ruptor Elite homogenizer (Omni International, USA), followed by centrifugation to collect the supernatant for cytokines analysis. The levels of inflammatory cytokines (IL-1β, TNF-α, and TGF-β1) in lung tissue homogenates and cell culture supernatants were quantified using ELISA kits according to the manufacturer's protocols. Briefly, samples and standards were added to pre-coated plates, followed by incubation with detection antibodies and streptavidin–HRP. Color development was achieved using 3,3′,5,5′-tetramethylbenzidine (TMB) substrate, and absorbance was measured at 450 nm with a microplate reader.

Hydroxyproline Assay

Lung collagen content was quantified using a HYP assay kit (Solarbio, BC0250). Briefly, 30 mg of lung tissue was hydrolyzed in 1 mL hydrolysis solution at 100 °C for 20 min, neutralized, and diluted to 10 mL. After charcoal treatment and centrifugation, the supernatant was analyzed at 550 nm using a microplate reader. HYP levels were calculated from a standard curve.

Statistical Analysis

All quantitative data are expressed as mean ± SD. Statistical significance was evaluated using GraphPad Prism 9.0. Two-group comparisons were analyzed by unpaired two-tailed Student's t-tests, and multiple comparisons were conducted using one-way ANOVA followed by Tukey's post hoc test. Survival curves were compared using the log-rank (Mantel–Cox) test. A p value < 0.05 was considered statistically significant.

Results

Preparation and Characterization of DHA@HSA and NIN@HSA Nanoparticles

Biocompatible DHA@HSA and NIN@HSA nanoparticles were successfully fabricated via a self-assembly strategy based on the co-solvent system of DMSO, anhydrous ethanol, and deionized water, with HSA serving as the carrier matrix (Figure 1A). TEM imaging revealed that both formulations exhibited uniformly distributed spherical morphologies with smooth surfaces (Figure 1B and C). DLS confirmed monodisperse size distributions, with mean hydrodynamic

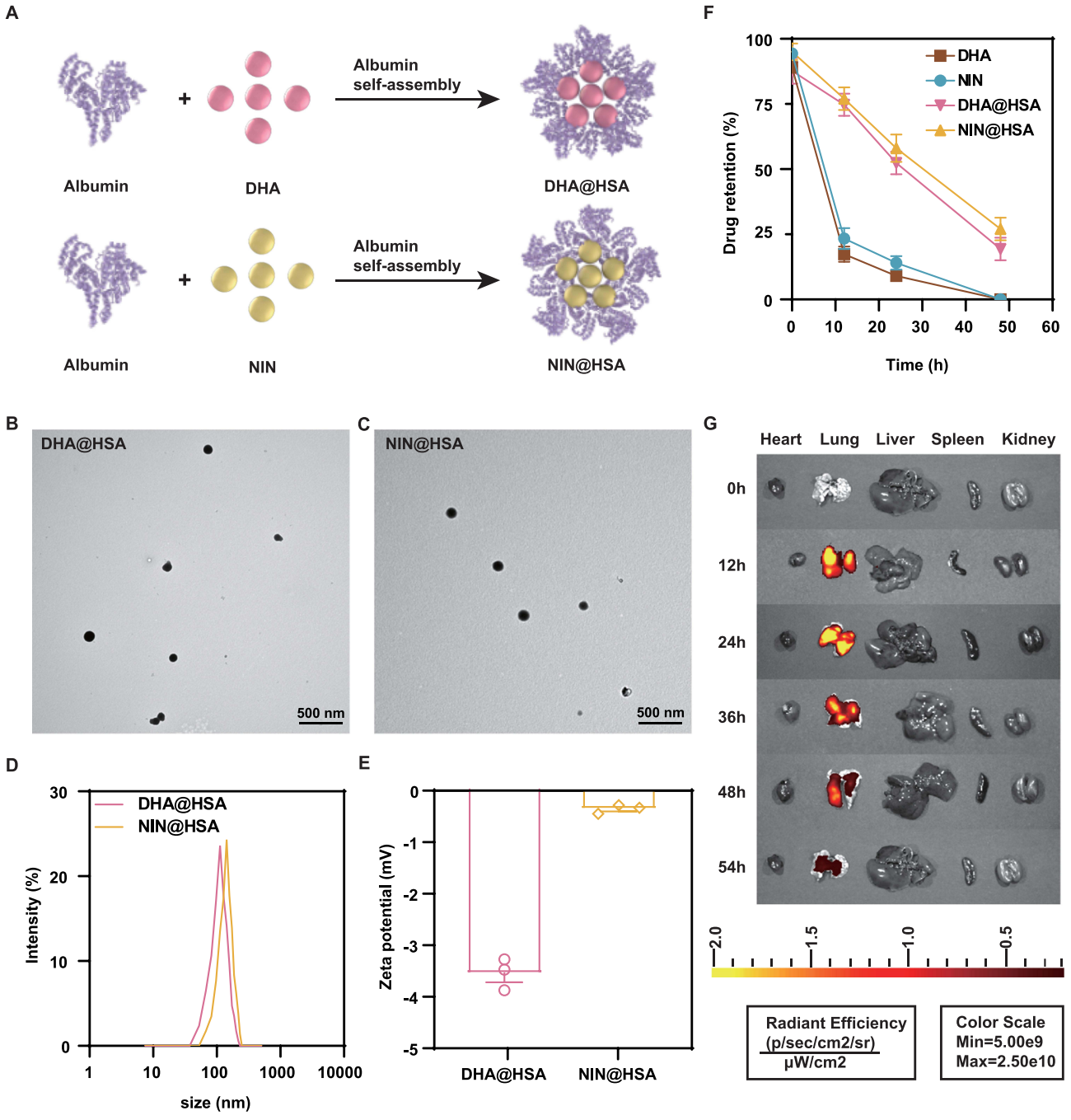

Figure 1 Preparation, characterization, and pulmonary retention of albumin nanoparticles. (**A**) Schematic illustration of the preparation process of DHA@HSA and NIN@HSA nanoparticles via a self-assembly method. (**B** and **C**) Transmission electron microscopy (TEM) images showing uniformly dispersed spherical morphologies of DHA@HSA and NIN@HSA nanoparticles. (**D** and **E**) Hydrodynamic size distributions and zeta potential values of nanoparticles determined by dynamic light scattering (DLS) (n = 3). (**F**) Pulmonary retention of free DHA, free NIN, DHA@HSA and NIN@HSA at different time points post-inhalation (n = 3). (**G**) Representative in vivo fluorescence images of Cy7-labeled DHA/NIN@HSA nanoparticles at 0–54 h after airway inhalation.

https://doi.org/10.2147/IJN.S576680

diameters of approximately 120 nm for DHA@HSA and 130 nm for NIN@HSA (Figure 1D). The zeta potentials were −3.5 mV and −0.3 mV, respectively, suggesting near-neutral to slightly negative surface charges (Figure 1E). As shown in Figure S1, both DHA@HSA and NIN@HSA nanoparticles exhibited good stability in PBS (pH 7.4) at 37°C over 48 h, maintaining consistent hydrodynamic diameters and low PDI values, while demonstrating a controlled release profile. The drug loading efficiencies of DHA and NIN were determined to be approximately 6.6% and 5.8%, respectively, which were sufficient to ensure stable drug incorporation and therapeutic availability.

To assess the pulmonary targeting and retention behavior of the inhalable nanoparticles, mice were administered free DHA, free NIN, DHA@HSA, or NIN@HSA, via airway inhalation. Lung tissues were collected at 12, 24, and 48 h post-administration, and the concentrations of DHA and NIN were quantified using HPLC and UV–Vis spectrophotometry, respectively. Quantitative analyses showed that free DHA and NIN were rapidly cleared within 12 h, whereas approximately 23% of DHA@HSA and NIN@HSA remained in the lungs after 48 h (Figures 1F, S2–4, and Table S1). Strikingly, in vivo fluorescence imaging of Cy7-labeled DHA/NIN@HSA nanoparticles revealed strong and sustained signals confined to the lungs, with no detectable fluorescence observed in other organs up to 48 h post-administration (Figure 1G). These findings confirm that HSA-based nanoparticles significantly improve pulmonary targeting and retention efficiency, thereby enhancing local drug bioavailability while minimizing systemic exposure.

Drug-Loaded Albumin Nanoparticles Inhibit TGF-β1–Induced Fibroblast Activation and Differentiation in vitro

The TGF-β1 signaling pathway is a central regulator in PF, driving fibroblast activation and excessive ECM deposition.[27,28] To investigate the inhibitory effects of DHA/NIN@HSA on fibroblast differentiation, NIH/3T3 cells were first stimulated with 10 ng/mL TGF-β1 for 48 h to induce activation.[29] Prior to evaluating anti-fibrotic effects, the cytotoxicity of co-delivered DHA@HSA and NIN@HSA nanoparticles was assessed in NIH/3T3 cells using the CCK-8 assay at varying concentration combinations. As shown in Figure S5, the combination of 1 μg/mL DHA and 0.5 μg/mL NIN maintained over 80% cell viability and was therefore selected for subsequent experiments. TGF-β1–activated fibroblasts were then treated with free NIN, free DHA, free DHA/NIN combination, NIN@HSA, DHA@HSA, or DHA/NIN@HSA. Immunofluorescence staining was performed to assess the expression of Collagen I and α-SMA, key markers of fibroblast activation and hallmarks of PF. As expected, TGF-β1 stimulation markedly enhanced Collagen I and α-SMA expression compared with PBS controls (Figure 2A–C), confirming successful fibroblast activation. All drug-treated groups exhibited varying degrees of signal reduction. NIN@HSA further decreased Collagen I and α-SMA levels compared with free NIN, while DHA@HSA outperformed free DHA. Notably, the DHA/NIN@HSA combination achieved the greatest suppression, exceeding the effect of the free DHA/NIN combination and approaching baseline levels observed in the PBS group. Importantly, the inhibitory effect of DHA@HSA alone was comparable to that observed for NIN@HSA. These trends were corroborated by qPCR analysis, where mRNA expression of Collagen I and α-SMA was significantly reduced in the DHA/NIN@HSA group (Figure 2D and E).

To examine whether the nanoparticles also modulate fibroblast-mediated inflammation, IL-1β and TNF-α levels were measured by ELISA. TGF-β1–activated NIH/3T3 cells exhibited pronounced elevation of both cytokines (Figure 2F and G). Whereas NIN or NIN@HSA showed limited effects on cytokine production, DHA or DHA@HSA significantly reduced IL-1β and TNF-α levels. Strikingly, the combined DHA@HSA and NIN@HSA treatment elicited the strongest suppression, indicating superior anti-inflammatory activity of the dual nanoparticle formulation. Given that inflammatory mediators can amplify profibrotic signaling and reinforce TGF-β1 activation, this pronounced cytokine attenuation may contribute to the enhanced inhibition of fibroblast activation and ECM-related markers in the co-delivery group.

Collectively, these results indicate that DHA/NIN@HSA nanoparticles not only suppress TGF-β1–induced fibroblast activation and differentiation but also attenuate proinflammatory cytokine secretion, highlighting their potential for targeted antifibrotic therapy.

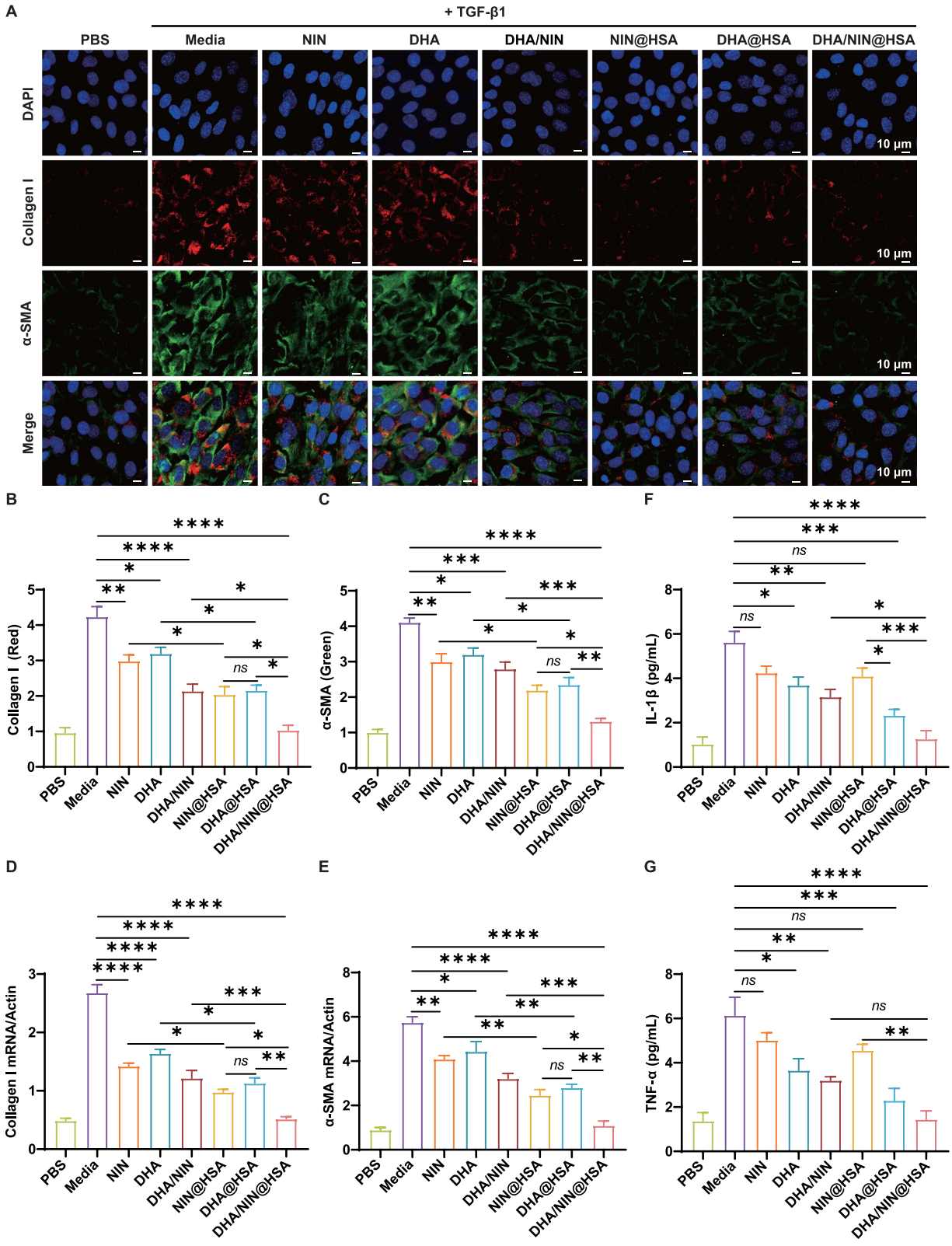

Figure 2 DHA/NIN@HSA inhibit TGF-β1-induced fibroblast activation and proinflammatory cytokine secretion in vitro. (**A**) Representative immunofluorescence images showing Collagen I and alpha-smooth muscle actin (α-SMA) expression in NIH/3T3 cells treated with PBS, TGF-β1, free NIN, free DHA, free DHA/NIN, NIN@HSA, DHA@HSA, or DHA/NIN@HSA (scale bar: 10 μm). (**B** and **C**) Quantification of immunofluorescence intensity for Collagen I (**B**) and α-SMA (**C**) in NIH/3T3 cells after indicated treatments (n = 3). (**D** and **E**) mRNA expression levels of Collagen I (**D**) and α-SMA (**E**) analyzed by qPCR (n = 3). (**F** and **G**) Secretion of IL-1β (**F**) and TNF-α (**G**) measured by ELISA (n = 3). ns, not significant; $p \geq 0.05$; *$p < 0.05$, **$p < 0.01$, ***$p < 0.001$, and ****$p < 0.0001$ (one-way ANOVA). Data are presented as mean ± standard deviation (SD).

https://doi.org/10.2147/IJN.S576680

Therapeutic Efficacy of DHA/NIN@HSA in vivo

Building on the in vitro findings that DHA/NIN@HSA significantly mitigates TGF-β1–induced fibroblast activation, we evaluated its therapeutic efficacy in vivo using a BLM-induced PF mouse model. C57BL/6 mice received an intratracheal instillation of BLM (2.5 mg/kg) to induce PF. Seven days after BLM instillation, mice received intratracheal microspray administration of PBS, NIN@HSA, DHA@HSA, or DHA/NIN@HSA, with doses of 4 mg/kg NIN and 2 mg/kg DHA every 48 h for a total of seven treatments (Figure 3A).

Body weight was monitored throughout the study as a general indicator of health and disease progression. Mice in the BLM-treated group (G2) exhibited rapid weight loss with minimal recovery, whereas healthy controls (G1) gained weight steadily. Both NIN@HSA (G3) and DHA@HSA (G4) partially mitigated weight loss, demonstrating comparable therapeutic effects, suggesting that DHA monotherapy exhibits antifibrotic efficacy comparable to NIN. Notably, mice receiving the combined DHA/NIN@HSA treatment (G5) experienced the least weight loss and the fastest recovery, indicating superior in vivo efficacy (Figure 3B). Survival analysis further corroborated these findings in the predefined survival cohort (n = 6 per group) (Figure 3C). Marked mortality was observed in the BLM group, whereas survival was improved in the treatment groups. Notably, no mortality was observed in either the healthy control group (G1) or the DHA/NIN@HSA group (G5) during the 21-day observation period, resulting in overlapping survival curves. For endpoint analyses, lung tissues, BALF, and serum were collected on Day 21 from randomly selected mice (n = 6 per group) as described in the Methods.

Histological and quantitative analyses were performed using MT staining and modified Ashcroft scoring to evaluate lung architecture and fibrosis severity.[30] BLM administration induced extensive structural distortion, collagen deposition, and elevated fibrosis scores in G2, confirming successful model establishment (Figure 3D and E). Quantification of HYP content showed a marked increase in G2 compared with G1, partial reductions in G3 and G4, and the most substantial decrease in G5 (Figure 3F). Moreover, collagen intensity quantified from MT-stained images was reduced across all treatment groups, with the greatest improvement observed in the DHA/NIN@HSA group (G5) (Figure 3G). These results indicate that combined DHA/NIN@HSA treatment effectively suppresses fibrotic matrix accumulation in vivo.

To visualize lung structural recovery, micro-CT imaging and 3D reconstructions were conducted on day 21 post-BLM challenge. Lungs from G2 mice displayed severe architectural distortion, irregular surfaces, and airspace collapse (Figure 4A). In contrast, NIN@HSA (G3) and DHA@HSA (G4) partially restored normal architecture, whereas DHA/NIN@HSA (G5) achieved near-complete recovery, closely resembling the healthy control group. Quantitative 3D lung volume analysis confirmed significant improvement in G5, with values approaching those of G1 (Figure 4B). These data demonstrate that inhaled DHA/NIN@HSA nanoparticles markedly restore pulmonary structure following fibrotic injury.

Immunofluorescence staining revealed robust expression of α-SMA and Collagen I in BLM-treated lungs (G2), indicating extensive fibroblast activation and ECM accumulation (Figure 4C–E). Treatment with NIN@HSA (G3) or DHA@HSA (G4) markedly suppressed these fibrotic markers, with comparable efficacy between the two. Importantly, DHA/NIN@HSA (G5) produced the most pronounced reduction, nearly restoring basal expression levels. BALF analysis showed significantly elevated total protein concentrations in G2, reflecting alveolar barrier disruption, while DHA/NIN@HSA treatment (G5) markedly reduced these levels (Figure S6). In parallel, ELISA of lung homogenates revealed elevated IL-1β, TNF-α, and TGF-β1 in G2, which were substantially decreased in G5 (Figure 4F–H). Collectively, these findings demonstrate that inhaled DHA/NIN@HSA nanoparticles effectively attenuate PF by reducing fibroblast activation, collagen deposition, and inflammatory cytokines release.

To assess the systemic safety of the treatment formulations, major organ histology and serum biochemical parameters were evaluated across all groups. H&E staining revealed no discernible histopathological abnormalities in the heart, liver, spleen, or kidneys of any treated mice (Figure 5A). Consistent with these findings, serum levels of ALT (Figure 5B) and AST (Figure S7A) showed no significant differences among the groups, indicating the absence of hepatic toxicity. Similarly, BUN levels remained stable across all treatment conditions (Figure S7B), suggesting preserved renal function. Furthermore, throughout the study period, no additional AEs—such as abnormal behaviors, weight fluctuations beyond expected ranges, or unexpected organ pathology—were observed. These results collectively confirm the favorable biocompatibility and in vivo safety of DHA/NIN@HSA nanoparticles. Given the significant antifibrotic and anti-inflammatory effects of DHA/NIN@HSA in vivo without observable systemic toxicity, we next explored the molecular mechanism underlying these therapeutic benefits.

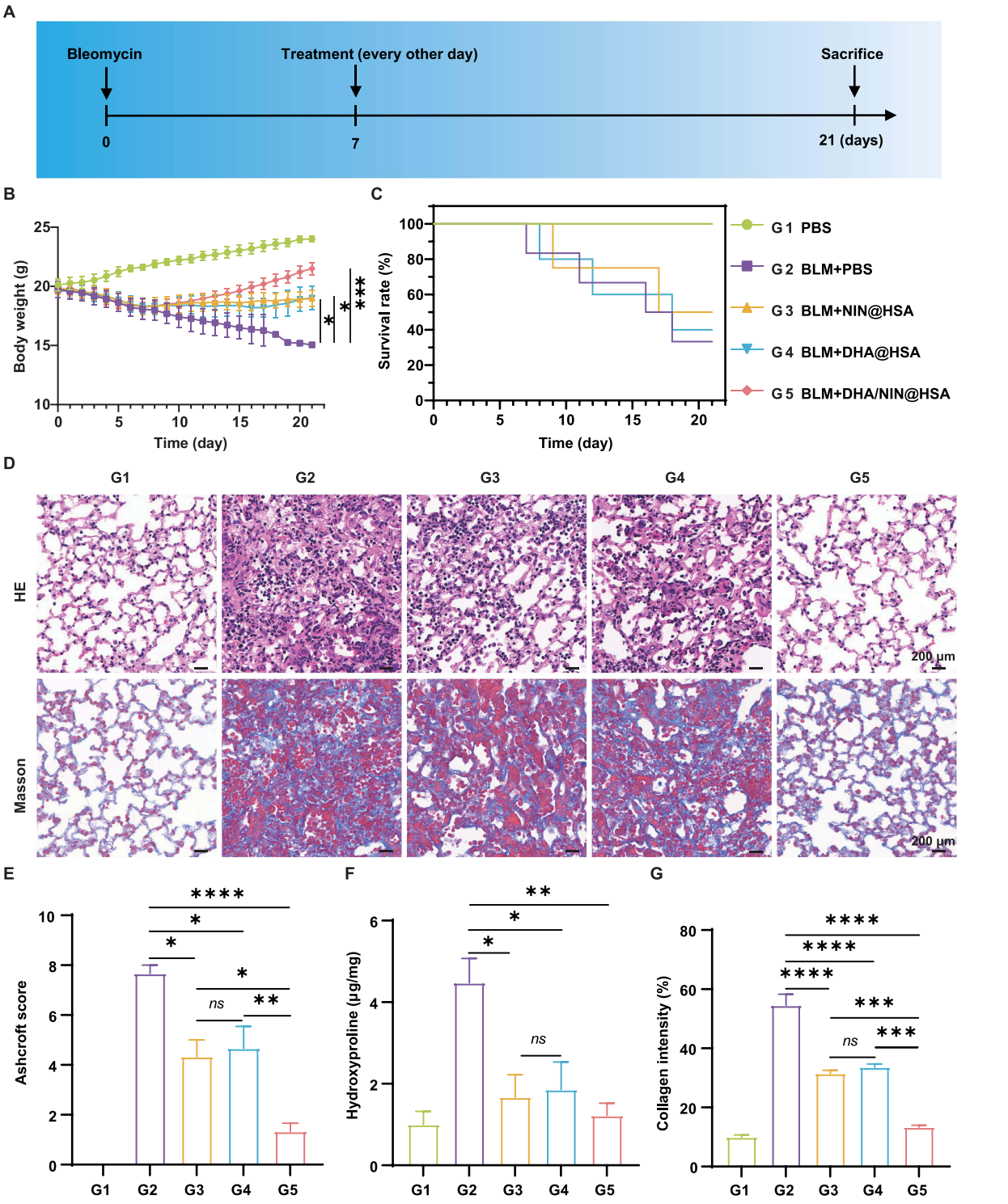

Figure 3 DHA/NIN@HSA improves survival and histopathological outcomes in a bleomycin-induced pulmonary fibrosis mouse model. (**A**) Schematic illustration of the bleomycin-induced pulmonary fibrosis model and the subsequent treatment protocol via airway administration. C57BL/6 mice were intratracheally instilled with bleomycin (2.5 mg/kg) to induce pulmonary fibrosis, followed by intratracheal administration of PBS, NIN@HSA, DHA@HSA, or DHA/NIN@HSA every 48 h for seven treatments. (**B**) Body weight changes of mice in different groups over the course of the study. (**C**) Survival curves of mice after different treatments. Note: The survival curves of G1 and G5 completely overlap due to 100% survival in both groups during the observation period. Survival curves were compared using the Kaplan–Meier method with the log-rank (Mantel–Cox) test. (**D**) Representative images of hematoxylin and eosin (H&E) and Masson's trichrome (MT) staining in lung tissues (scale bar: 200 μm). (**E**) Modified Ashcroft scores of lung sections in different treatment groups. (**F**) Hydroxyproline (HYP) content in lung tissues after different treatments. (**G**) Quantification of collagen intensity in lung tissues from MT-stained images across different groups. To account for the expected mortality in the bleomycin model, three parallel sets of experiments (6 mice per group in each set) were conducted under identical conditions (modeled and treated on the same day using the same reagent batches). Survival analysis in (**C**) was performed using one predefined set (n = 6 per group). For endpoint analyses in (**B**) and (**D**–**G**), 6 mice per group were randomly selected from the pooled animals across the remaining sets. G1: healthy control group; G2: bleomycin model group; G3: NIN@HSA group; G4: DHA@HSA group; G5: DHA/NIN@HSA group. ns, not significant; $p \geq 0.05$; *$p < 0.05$, **$p < 0.01$, ***$p < 0.001$, and ****$p < 0.0001$. Data are presented as mean ± standard deviation (SD). Endpoint comparisons were performed using one-way ANOVA.

https://doi.org/10.2147/IJN.S576680

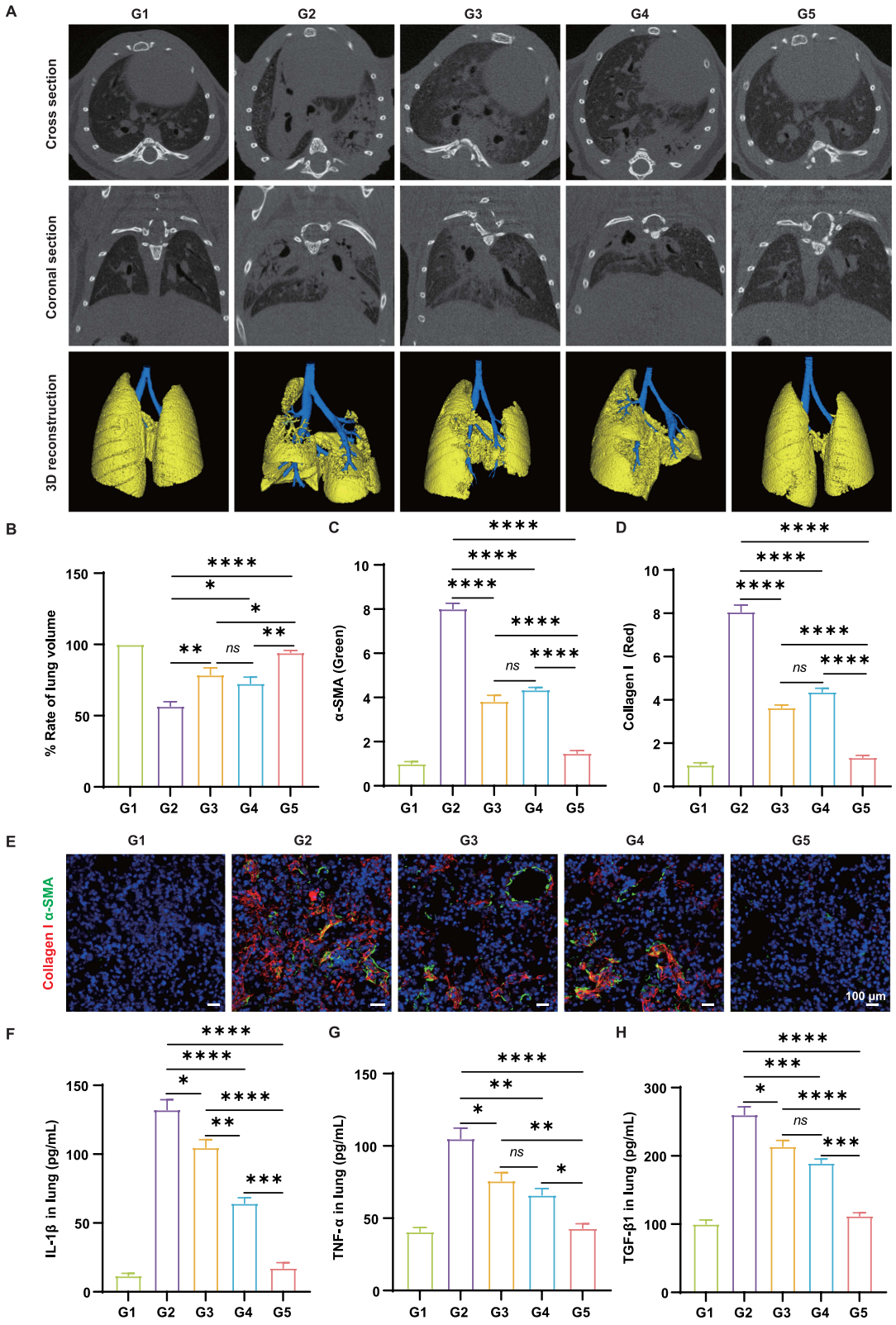

Figure 4 DHA/NIN@HSA improve lung structure and suppress fibrosis and inflammation in vivo. (**A**) Representative micro-computed tomography (micro-CT) images, three-dimensional (3D) reconstructions, and lung photographs of G1–G5 mice collected 21 days after bleomycin administration. (**B**) Quantitative analysis of 3D lung volume derived from micro-CT scans. (**C** and **D**) Representative immunofluorescence images and quantification of α-SMA (**C**) and Collagen I (**D**) expression in lung tissues (scale bar: 100 μm). (**E**) Distribution of α-SMA (green) and Collagen I (red) in lung sections from different treatment groups. (**F–H**) Levels of proinflammatory and profibrotic cytokines (IL-1β, TNF-α, and TGF-β1) in lung tissue homogenates measured by ELISA. G1: healthy control group; G2: bleomycin model group; G3: NIN@HSA group; G4: DHA@HSA group; G5: DHA/NIN@HSA group. ns, not significant; $p \geq 0.05$; *$p < 0.05$, **$p < 0.01$, ***$p < 0.001$, and ****$p < 0.0001$ (one-way ANOVA). Data are presented as mean ± standard deviation (SD) (n = 6).

https://doi.org/10.2147/IJN.S576680

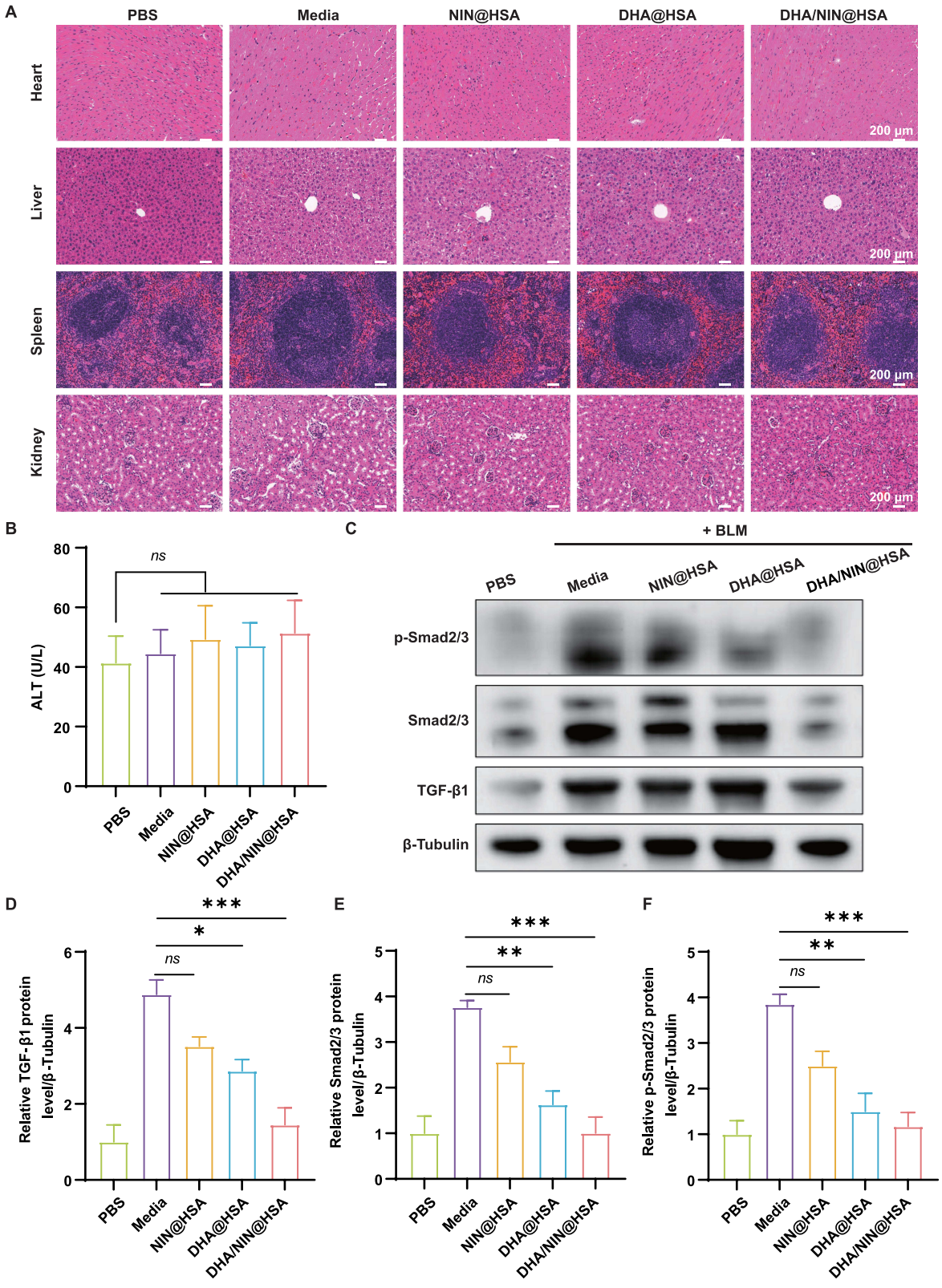

Figure 5 DHA/NIN@HSA inhibits TGF-β1/Smad2/3 signaling activation and exhibits excellent biosafety in vivo. (**A**) Representative hematoxylin and eosin (H&E)-stained images of major organs (heart, liver, spleen, and kidney) from various groups (scale bar: 200 μm). (**B**) Serum alanine aminotransferase (ALT) levels in mice after different treatments (n = 6). (**C**–**F**) Western blot (WB) analysis and quantitative results of TGF-β1, Smad2/3, and phosphorylated Smad2/3 (p-Smad2/3) expression levels in lung tissues from different treatment groups (n = 3). ns, not significant; $p \geq 0.05$; *$p < 0.05$, **$p < 0.01$, and ***$p < 0.001$ (one-way ANOVA). Data are presented as mean ± standard deviation (SD).

https://doi.org/10.2147/IJN.S576680

DHA/NIN@HSA Nanoparticles Attenuate PF via Suppression of TGF-β1/Smad2/3 Signaling

The TGF-β1/Smad2/3 signaling cascade is a pivotal driver of fibroblast activation and ECM accumulation during PF.[27] Persistent activation of this pathway drives the transcription of profibrotic genes such as *α-SMA* and *Collagen I*, thereby contributing to irreversible tissue remodeling.[31] To further clarify the mechanism underlying the observed antifibrotic effects, we examined whether DHA/NIN@HSA treatment modulates this signaling axis in vivo.

Lung tissues harvested on day 21 post-BLM administration were analyzed by WB for TGF-β1, Smad2/3, and p-Smad2/3. Compared with the BLM group (G2), all treatment groups showed reduced expression of TGF-β1, Smad2/3, and p-Smad2/3 (Figure 5C–F). The inhibitory effect was most pronounced in the DHA/NIN@HSA group (G5), in which these protein levels were reduced to near-baseline levels comparable to healthy controls. DHA@HSA (G4) also markedly downregulated the pathway, whereas NIN@HSA (G3) exerted a moderate inhibitory effect. Notably, the extent of TGF-β1/Smad2/3 suppression paralleled the overall therapeutic outcomes. The dual DHA/NIN@HSA treatment (G5) produced the strongest reduction in TGF-β1 and p-Smad2/3, accompanied by the greatest decreases in fibrotic markers (α-SMA and Collagen I) and inflammatory cytokines (IL-1β and TNF-α). Collectively, these findings suggest that DHA and NIN exert complementary actions in vivo. DHA primarily attenuates inflammation-associated and TGF-β1/Smad2/3–driven profibrotic signaling, whereas NIN further limits fibroblast activation and fibrotic remodeling, resulting in enhanced antifibrotic efficacy upon co-delivery.

Discussion

PF is a chronic, progressive disease with exceptionally high mortality, characterized by irreversible scarring of lung tissue. Without timely intervention, patients typically succumb to respiratory failure. Although PFD and NIN have been approved by the FDA and can slow disease progression to some extent,[7,10] their therapeutic efficacy remains limited due to disease heterogeneity, insufficient potency, and dose-related AEs.[1] These challenges underscore the urgent need for novel therapeutic strategies capable of addressing both inflammatory and fibrotic processes.

In the early stages of PF, infiltration of cytokines and chemokines recruit macrophages and neutrophils, triggering innate and adaptive immune responses. This immune activation amplifies the inflammatory cascade, thereby accelerating fibrogenesis.[32,33] TGF-β1 acts as a central regulator that promotes fibroblast-to-myofibroblast transformation.[27,28] Activated myofibroblasts excessively deposit ECM and collagen while releasing IL-1β, TNF-α, and TGF-β1, creating a vicious cycle of inflammation and fibrosis.[34] Therefore, simultaneous inhibition of inflammatory and fibrotic pathways may offer a more effective therapeutic approach.

Albumin-based nanoparticles are designed to maintain structural integrity under physiological conditions while enabling controlled drug release. In this study, we developed an inhalable HSA-based nanoparticle delivery system co-delivering DHA and NIN to overcome the limitations of conventional oral therapy. Both DHA@HSA and NIN@HSA nanoparticles exhibited stable hydrodynamic diameters and consistently low PDI values (~0.12) in PBS (pH 7.4) over 48 h incubation period, demonstrating good colloidal stability. The corresponding in vitro release profiles were characterized by an initial moderate release followed by a pronounced deceleration in release rate, reaching approximately 40% cumulative release at 48 h. Such release behavior is generally consistent with previously reported albumin-based nanocarrier systems,[35] in which partial and stabilized drug release under physiological conditions is generally regarded as an indicator of formulation stability. In vivo fluorescence imaging demonstrated strong pulmonary accumulation with negligible distribution in other major organs, indicating pronounced lung-targeting capability of albumin nanoparticles upon airway administration. This property enables local drug enrichment in fibrotic regions, enhancing therapeutic efficacy while minimizing systemic exposure.

Albumin has been widely exploited as a drug carrier, with clear clinical precedent: for example, albumin-bound paclitaxel (an FDA-approved formulation) improved solubility and clinical outcomes in advanced breast and pancreatic cancers.[36,37] Other preclinical studies have documented marked solubility and bioavailability gains for lipophilic agents formulated with HSA.[38] Although these examples derive from systemic applications rather than inhalation, they validate HSA's capacity to enhance solubility, stabilize labile drugs, and facilitate translational development. Together with our

biodistribution results, these findings strongly support HSA as an ideal platform for pulmonary delivery of DHA and NIN, enabling enhanced local bioavailability and sustained lung retention while minimizing systemic exposure. These features may help address common limitations of inhaled antifibrotic formulations, such as rapid pulmonary clearance and limited local residence time, thereby supporting sustained local drug exposure in fibrotic lungs. Despite these promising attributes, the clinical translation of HSA-based inhalation carriers faces challenges that warrant further consideration. A primary hurdle lies in the complexity and cost of industrial scale-up.[39] Unlike synthetic polymers, HSA is a natural protein prone to batch-to-batch variability; consequently, rigorous quality control during large-scale manufacturing is essential to ensure the reproducibility of particle size and drug loading. Furthermore, albumin nanoparticles may be susceptible to aggregation or premature drug leakage during long-term storage or the intratracheal administration process.[40] Finally, although albumin possesses a favorable biocompatibility profile, pulmonary administration warrants a systematic assessment of local tolerability and potential immunological responses. Importantly, many of these issues are not unique to albumin-based systems and can be addressed through formulation optimization and standardized manufacturing controls. Addressing these challenges will further support the clinical feasibility of inhalable HSA-based nanomedicines.

We successfully prepared DHA@HSA and NIN@HSA nanoparticles with uniform size, a near-neutral to slightly negative surface charge, and satisfactory encapsulation efficiency, supporting good colloidal stability and pulmonary deposition. When evaluated individually, DHA exhibited antifibrotic efficacy comparable to NIN while exerting stronger anti-inflammatory effects, suggesting that DHA monotherapy is a promising candidate for fibrosis therapy. More importantly, in vitro co-delivery of DHA@HSA and NIN@HSA significantly decreased IL-1β and TNF-α secretion and suppressed α-SMA and Collagen I expression in TGF-β1–stimulated fibroblasts, confirming both anti-inflammatory and antifibrotic activities. Consistently, in vivo administration of the combined system alleviated BLM-induced PF, as reflected by improved body weight recovery, prolonged survival, and reduced pulmonary expression of IL-1β, TNF-α, TGF-β1, α-SMA, and Collagen I. Micro-CT 3D reconstruction further confirmed substantial restoration of lung architecture. Collectively, these findings demonstrate that airway co-delivery of DHA@HSA and NIN@HSA yields the most pronounced antifibrotic efficacy and favorable safety profile, attributable to the complementary pharmacological actions of the two agents.

Mechanistically, NIN, as a multitarget receptor tyrosine kinase inhibitor, has been reported to suppress fibroblast proliferation and myofibroblast differentiation.[10,11] DHA attenuates PF progression by inhibiting aberrant activation of the TGF-β1/Smad2/3 signaling pathway and reducing IL-1β and TNF-α levels. Previous studies have also shown that DHA alleviates oxidative stress during fibrosis.[16,17] Notably, inflammatory mediators have been implicated in amplifying profibrotic signaling and sustaining TGF-β1 activation, which may further promote fibroblast activation and ECM deposition.[41,42] Therefore, the pronounced cytokine attenuation observed in the co-delivery group may, at least in part, contribute to its enhanced inhibition of fibrotic remodeling. Collectively, the complementary actions of DHA and NIN enable intervention at both inflammatory and fibrotic stages, potentially resulting in improved therapeutic efficacy compared with monotherapy.

In summary, the inhalable co-delivery system of DHA@HSA and NIN@HSA enables precise pulmonary targeting, sustained lung retention, and concurrent suppression of fibrotic and inflammatory processes, with no detectable histopathological abnormalities in major organs. This strategy represents a safe and effective therapeutic avenue for PF, offering strong potential for future clinical translation.

Conclusion

This study demonstrates that DHA exhibits antifibrotic efficacy comparable to NIN and superior anti-inflammatory activity, highlighting its potential as a therapeutic agent for PF. Furthermore, the inhalable HSA-based nanoparticle system co-delivering DHA@HSA and NIN@HSA achieved precise pulmonary targeting, significantly attenuated BLM-induced fibrosis, and showed excellent safety. Mechanistically, co-delivery enhances efficacy through the synergistic integration of DHA-mediated suppression of inflammatory responses and the TGF-β1/Smad2/3 signaling axis with NIN-mediated inhibition of fibroblast activation and fibrotic remodeling. These findings support a safe, effective, and clinically translatable strategy for combination therapy of PF.

Data Sharing Statement

Data of this study are available from the corresponding author upon reasonable request.

Ethics Approval

Animal experimental procedures were approved by the Institutional Animal Care and Use Committee of the Institute of Process Engineering, Chinese Academy of Sciences (IPEAECA2024031). Mice were anesthetized with 1% pentobarbital sodium (50 mg/kg, intraperitoneally) prior to intratracheal procedures and euthanized with an overdose of pentobarbital sodium (150 mg/kg, intraperitoneally), in accordance with the American Veterinary Medical Association (AVMA) Guidelines for the Euthanasia of Animals (2020).

Acknowledgments

We thank the Institute of Process Engineering, Chinese Academy of Sciences for providing the platform for animal experiments.

Author Contributions

All authors made a significant contribution to the work reported, whether that is in the conception, study design, execution, acquisition of data, analysis and interpretation, or in all these areas; took part in drafting, revising or critically reviewing the article; gave final approval of the version to be published; have agreed on the journal to which the article has been submitted; and agree to be accountable for all aspects of the work.

Disclosure

The authors report no conflicts of interest in this work.

References

1. Martinez FJ, Collard HR, Pardo A, et al. Idiopathic pulmonary fibrosis. *Nat Rev Dis Primers*. 2017;3:17074. doi:10.1038/nrdp.2017.74
2. Lederer DJ, Martinez FJ. Idiopathic pulmonary fibrosis. *N Engl J Med*. 2018;378(19):1811–1823. doi:10.1056/NEJMra1705751
3. Maher TM, Bendstrup E, Dron L, et al. Global incidence and prevalence of idiopathic pulmonary fibrosis. *Respir Res*. 2021;22(1):197. doi:10.1186/s12931-021-01791-z
4. Richeldi L, Collard HR, Jones MG. Idiopathic pulmonary fibrosis. *Lancet*. 2017;389(10082):1941–1952. doi:10.1016/S0140-6736(17)30866-8
5. Dove EP, Olson AL, Glassberg MK. Trends in idiopathic pulmonary fibrosis-related mortality in the United States: 2000-2017. *Am J Respir Crit Care Med*. 2019;200(7):929–931. doi:10.1164/rccm.201905-0958LE
6. Cox IA, Otahal P, de Graaff B, et al. Incidence, prevalence and mortality of idiopathic pulmonary fibrosis in Australia. *Respirology*. 2022;27(3):209–216. doi:10.1111/resp.14194
7. Podolanczuk AJ, Thomson CC, Remy-Jardin M, et al. Idiopathic pulmonary fibrosis: state of the art for 2023. *Eur Respir J*. 2023;61(4):2200957. doi:10.1183/13993003.00957-2022
8. Maher TM, Lancaster LH, Jouneau S, et al. Pirfenidone treatment in individuals with idiopathic pulmonary fibrosis: impact of timing of treatment initiation. *Ann Am Thorac Soc*. 2019;16(7):927–930. doi:10.1513/AnnalsATS.201810-720RL
9. Nathan SD, Costabel U, Glaspole I, et al. Efficacy of pirfenidone in the context of multiple disease progression events in patients with idiopathic pulmonary fibrosis. *Chest*. 2019;155(4):712–719. doi:10.1016/j.chest.2018.11.008
10. Wind S, Schmid U, Freiwald M, et al. Clinical pharmacokinetics and pharmacodynamics of nintedanib. *Clin Pharmacokinet*. 2019;58(9):1131–1147. doi:10.1007/s40262-019-00766-0
11. Wollin L, Wex E, Pautsch A, et al. Mode of action of nintedanib in the treatment of idiopathic pulmonary fibrosis. *Eur Respir J*. 2015;45(5):1434–1445. doi:10.1183/09031936.00174914
12. Bermudo-Peloche G, Del Rio B, Vicens-Zygmunt V, et al. Pirfenidone in post-COVID-19 pulmonary fibrosis (FIBRO-COVID): a Phase 2 randomised clinical trial. *Eur Respir J*. 2025;65(4):2402249. doi:10.1183/13993003.02249-2024
13. Tu J, Chen X, Li C, et al. Nintedanib mitigates radiation-induced pulmonary fibrosis by suppressing epithelial cell inflammatory response and inhibiting fibroblast-to-myofibroblast transition. *Int J Biol Sci*. 2024;20(9):3353–3371. doi:10.7150/ijbs.92620
14. Inoue Y, Wells AU, Song JW, et al. Nintedanib in Asian patients with progressive fibrosing interstitial lung diseases: results from the INBUILD trial. *Respirology*. 2023;28(5):465–474. doi:10.1111/resp.14452
15. Zheng YJ, Li X, Sun L, Guo JW. Therapeutic effect of dihydroartemisinin on pulmonary fibrosis in rats with dust. *Zhonghua Lao dong wei sheng zhi ye bing za zhi*. 2019;37(2):96–103. doi:10.3760/cma.j.issn.1001-9391.2019.02.003
16. Yang D-X, Qiu J, Zhou -H-H, et al. Dihydroartemisinin alleviates oxidative stress in bleomycin-induced pulmonary fibrosis. *Life Sci*. 2018;205:176–183. doi:10.1016/j.lfs.2018.05.022
17. Yang D, Yuan W, Lv C, et al. Dihydroartemisinin supresses inflammation and fibrosis in bleomycine-induced pulmonary fibrosis in rats. *Int J Clin Exp Pathol*. 2015;8(2):1270–1281.

18. Richeldi L, Costabel U, Selman M, et al. Efficacy of a tyrosine kinase inhibitor in idiopathic pulmonary fibrosis. *New Engl J Med*. 2011;365(12):1079–1087. doi:10.1056/NEJMoa1103690
19. Richeldi L, du Bois RM, Raghu G, et al. Efficacy and safety of nintedanib in idiopathic pulmonary fibrosis. *New Engl J Med*. 2014;370(22):2071–2082. doi:10.1056/NEJMoa1402584
20. West A, Chaudhuri N, Barczyk A, et al. Inhaled pirfenidone solution (AP01) for IPF: a randomised, open-label, dose-response trial. *Thorax*. 2023;78(9):882–889. doi:10.1136/thorax-2022-219391
21. Shi T, Jin M, Li H, et al. Inhaled nintedanib dry powder formulation for the treatment of idiopathic pulmonary fibrosis: pharmacodynamic and pharmacokinetic study. *Int J Pharm*. 2025;683:126088. doi:10.1016/j.ijpharm.2025.126088
22. Meng R, Hao S, Sun C, et al. Reverse-QTY code design of active human serum albumin self-assembled amphiphilic nanoparticles for effective anti-tumor drug doxorubicin release in mice. *Proc Natl Acad Sci U S A*. 2023;120(21):e2220173120. doi:10.1073/pnas.2220173120
23. Ullah A, Shin G, Lim SI. Human serum albumin binders: a piggyback ride for long-acting therapeutics. *Drug Discov Today*. 2023;28(10):103738. doi:10.1016/j.drudis.2023.103738
24. Akbarian A, Ebtekar M, Pakravan N, Hassan ZM. Folate receptor alpha targeted delivery of artemether to breast cancer cells with folate-decorated human serum albumin nanoparticles. *Int J Biol Macromol*. 2020;152:90–101.
25. Li D, Zhao A, Zhu J, et al. Inhaled lipid nanoparticles alleviate established pulmonary fibrosis. *Small*. 2023;19(30):e2300545. doi:10.1002/smll.202300545
26. Wang Y, Wang A, Zhang M, et al. Artesunate attenuates airway resistance in vivo and relaxes airway smooth muscle cells in vitro via bitter taste receptor-dependent calcium signalling. *Exp Physiol*. 2018;104(2):231–243. doi:10.1113/EP086824
27. Zhou X-M, Wang G-L, Wang X-B, et al. GHK peptide inhibits bleomycin-induced pulmonary fibrosis in mice by suppressing TGFβ1/Smad-mediated epithelial-to-mesenchymal transition. *Front Pharmacol*. 2017;8:904. doi:10.3389/fphar.2017.00904
28. Miao Y, Li X, Yang Y, et al. Entrectinib ameliorates bleomycin-induced pulmonary fibrosis in mice by inhibiting TGF-β1 signaling pathway. *Int Immunopharmacol*. 2022;113(Pt B):109427. doi:10.1016/j.intimp.2022.109427
29. Lee WT, Lee H, Kim J, et al. Alveolar macrophage phagocytosis-evading inhaled microgels incorporating nintedanib-PLGA nanoparticles and pirfenidone-liposomes for improved treatment of pulmonary fibrosis. *Bioact Mater*. 2024;33:262–278. doi:10.1016/j.bioactmat.2023.11.005
30. Hübner R-H, Gitter W, El Mokhtari NE, et al. Standardized quantification of pulmonary fibrosis in histological samples. *Biotechniques*. 2008;44(4):507–517. doi:10.2144/000112729
31. Dou C, Liu Z, Tu K, et al. P300 acetyltransferase mediates stiffness-induced activation of hepatic stellate cells into tumor-promoting myofibroblasts. *Gastroenterology*. 2018;154(8):2209–2221.e14. doi:10.1053/j.gastro.2018.02.015
32. Chen Y-C, Cheng Y-K, Chen J-H, et al. Cardamonin attenuates phorbol 12-myristate 13-acetate-induced pulmonary inflammation in alveolar macrophages. *Food Chem Toxicol*. 2022;159:112761. doi:10.1016/j.fct.2021.112761
33. Mutsaers SE, Miles T, Prêle CM, Hoyne GF. Emerging role of immune cells as drivers of pulmonary fibrosis. *Pharmacol Ther*. 2023;252:108562. doi:10.1016/j.pharmthera.2023.108562
34. Torr EE, Ngam CR, Bernau K, Tomasini-Johansson B, Acton B, Sandbo N. Myofibroblasts exhibit enhanced fibronectin assembly that is intrinsic to their contractile phenotype. *J Biol Chem*. 2015;290(11):6951–6961. doi:10.1074/jbc.M114.606186
35. Lomis N, Westfall S, Farahdel L, Malhotra M, Shum-Tim D, Prakash S. Human serum albumin nanoparticles for use in cancer drug delivery: process optimization and in vitro characterization. *Nanomaterials*. 2016;6(6):116. doi:10.3390/nano6060116
36. Gradishar WJ, Tjulandin S, Davidson N, et al. Phase III trial of nanoparticle albumin-bound paclitaxel compared with polyethylated castor oil-based paclitaxel in women with breast cancer. *J Clin Oncol*. 2005;23(31):7794–7803. doi:10.1200/JCO.2005.04.937
37. Von Hoff DD, Ervin T, Arena FP, et al. Increased survival in pancreatic cancer with nab-paclitaxel plus gemcitabine. *N Engl J Med*. 2013;369(18):1691–1703. doi:10.1056/NEJMoa1304369
38. Saleh T, Soudi T, Shojaosadati SA. Aptamer functionalized curcumin-loaded human serum albumin (HSA) nanoparticles for targeted delivery to HER-2 positive breast cancer cells. *Int J Biol Macromol*. 2019;130:109–116. doi:10.1016/j.ijbiomac.2019.02.129
39. Murphy G, Brayden DJ, Cheung DL, Liew A, Fitzgerald M, Pandit A. Albumin-based delivery systems: recent advances, challenges, and opportunities. *J Control Release*. 2025;380:375–395. doi:10.1016/j.jconrel.2025.01.035
40. Qu N, Song K, Ji Y, et al. Albumin Nanoparticle-Based Drug Delivery Systems. *Int J Nanomed*. 2024;19:6945–6980. doi:10.2147/IJN.S467876
41. Fathimath Muneesa M, Shaikh SB, Jeena TM, Bhandary YP. Inflammatory mediators in various molecular pathways involved in the development of pulmonary fibrosis. *Int Immunopharmacol*. 2021;96:107608. doi:10.1016/j.intimp.2021.107608
42. Aumiller V, Balsara N, Wilhelm J, Günther A, Königshoff M. WNT/β-catenin signaling induces IL-1β expression by alveolar epithelial cells in pulmonary fibrosis. *Am J Respir Cell Mol Biol*. 2013;49(1):96–104. doi:10.1165/rcmb.2012-0524OC